Embedding a Ruthenium-Based Structural Mimic of the [Fe]-Hydrogenase Cofactor into Papain

Chandan Kr Barik, Rakesh Ganguly, Yongxin Li, Cédric Przybylski, Michèle Salmain, Weng Kee Leong

Embedding a Ruthenium-Based Structural Mimic of the [Fe]-Hydrogenase Cofactor into Papain

Chandan Kr Barik,[†] Rakesh Ganguly,[†] Yongxin Li,[†] Cédric Przybylski,[‡] Michèle Salmain,*[,‡] and Weng Kee Leong*[,†]

[†]Division of Chemistry & Biological Chemistry, Nanyang Technological University, 21 Nanyang Link, Singapore 637371, Singapore
[‡]Sorbonne Université, CNRS, Institut Parisien de Chimie Moléculaire (IPCM), 4 place Jussieu, F-75005 Paris, France

Supporting Information

ABSTRACT: We describe the synthesis of the ruthenacyclic carbamoyl complexes [Ru(2-NHC(O)C_5H_3NMe)$(CO)_2$(*o*,*o*-Me_2-C_6H_3S)(L)] (L = H_2O or MeCN), which have a labile water or acetonitrile ligand at their sixth coordination sites. Steric bulk around the ruthenium center is essential in preventing isomerization and dimerization, and embedding within papain can be achieved via coordination of its sole free cysteine residue. The observed chemistry parallels that of the natural [Fe]-hydrogenase.

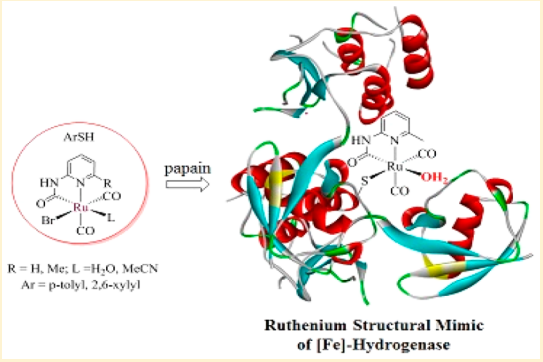

1. INTRODUCTION

Three distinct classes of hydrogenases are known, referred to as the [NiFe]-, [FeFe]-, and [Fe]-hydrogenases, and they all catalyze the reversible oxidation of dihydrogen into protons.[1−3] The redox-inactive [Fe]-hydrogenase, or H_2-forming methylene-tetrahydromethanopterin dehydrogenase (Hmd), takes part in the conversion of carbon dioxide to methane in many methanogenic archaea.[4] In particular, it catalyzes an intermediary step, which is the reversible and stereoselective reduction of a unique biological carbocationic substrate, N^5,N^{10}-methenyltetrahydromethanopterin (methenyl-H_4MPT$^+$), with dihydrogen to produce neutral methylenetetrahydromethanopterin (methylene-H_4MPT) and a proton (Scheme 1).[4−6]

Scheme 1. Reversible Reduction of Methenyl-H_4MPT$^+$

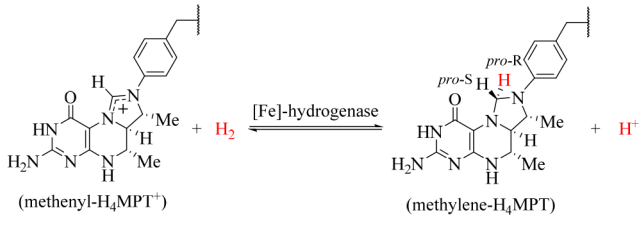

Crystallographic elucidation of the [Fe]-hydrogenase active site and its apoenzyme have been achieved, and the former comprises an iron(II) atom with pseudo-octahedral geometry;[7−10] it is bound to one cysteine residue, two mutually cis CO ligands, and a 2-acetyl-6-hydroxypyridinol ligand. The identity of the sixth ligand, *trans* to the acyl group, has not been confirmed, although it is most probably a water molecule (Figure 1a).[11−13] A number of Fe-based structural models of the active site have been reported over the years, including some which are also functional models.[14] In particular, Hu et al. recently showed that reconstitution of the entire [Fe]-hydrogenase using the apoenzyme produced in *E. coli* and an Fe-based model complex could activate dihydrogen.[15] That study points to a role for the protein in [Fe]-hydrogenase for the dihydrogen activation and that the pyridinyl cofactor most likely activates dihydrogen via coordination at the site *trans* to

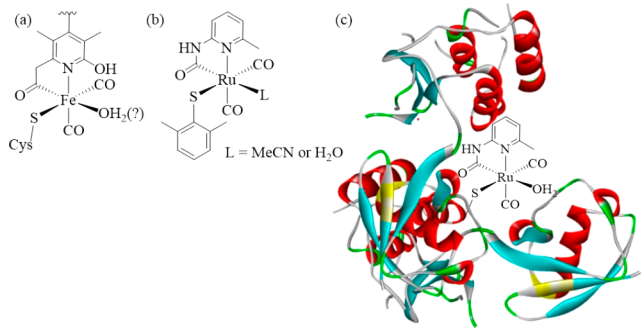

Figure 1. Structure of (a) the active site of [Fe]-hydrogenase, (b) ruthenium analogue of the active site of [Fe]-hydrogenase, and (c) ruthenium analogue of the entire enzyme synthesized in this study.

the acyl group. Such investigations are, nevertheless, hampered by the air-sensitivity of organoiron compounds.

We recently reported on the first ruthenium and osmium structural mimics for the [Fe]-hydrogenase active site.[16] Ruthenium complexes are generally more air-stable than their iron counterparts, and many are known to activate dihydrogen.[17,18] We therefore hypothesized that a reproduction of the [Fe]-hydrogenase using a more stable ruthenium model complex and an appropriate protein scaffold may serve as a useful model for studying aspects of its chemistry. Such metalloenzymes are also of interest as possibly possessing unique catalytic properties.[19] We chose papain as protein scaffold as it is readily and cheaply available, and its tertiary structure and chemistry are well-understood. In addition, it has a single free sulfhydryl (Cys25) moiety located in a pocket forming the enzyme's active site, which may allow binding to the ruthenium center in an analogous way to that present in native [Fe]-hydrogenase. Our investigations into this are presented here.

2. RESULTS AND DISCUSSION

Synthesis. The ruthenium-based structural mimics **3** can be synthesized in two steps from the corresponding ionic carbamoyl ruthenacycles **1** by following a recently reported procedure (Scheme 2).[16]

Scheme 2. Synthesis of 2 and 3

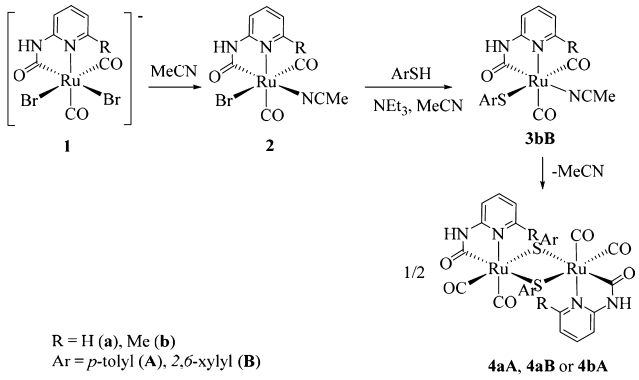

Unlike the iron analogue, thiolation of **2** requires the addition of a base.[14d] The mononuclear thiolato complexes **3** could be isolated only when the pyridine ligand is substituted at the 6-position, together with a bulky thiolate (**3bB**); dimerization occurs otherwise (**4aA**, **4aB**, and **4bA**). All the complexes **2**–**4** have been characterized spectroscopically and crystallographically; ORTEP plots of a representative of each are given in Figure 2.

The complexes **4** are sparingly soluble in dimethyl sulfoxide but not in other common organic solvents. All three are symmetrical Ru^{II}–Ru^{II} homodimers bridged by two thiolato ligands, but while **4aA** and **4aB** are centrosymmetric, the structure of **4bA** has approximate C_2 symmetry with the two tolyl groups (as are the two pyridyl groups) on the same side of the slightly puckered Ru_2S_2 ring. Their ^{1}H NMR spectra in d_6-DMSO show only one set of peaks; this is similar to the dimeric iron compound [{Fe(COMe)(CO)$_2$(μ^2-SPyMe)}$_2$].[14b] As in the case of the iron analogues, attempts to cleave the Ru–S bridges with phosphines (PMe_3 and PPh_3) failed.[14d]

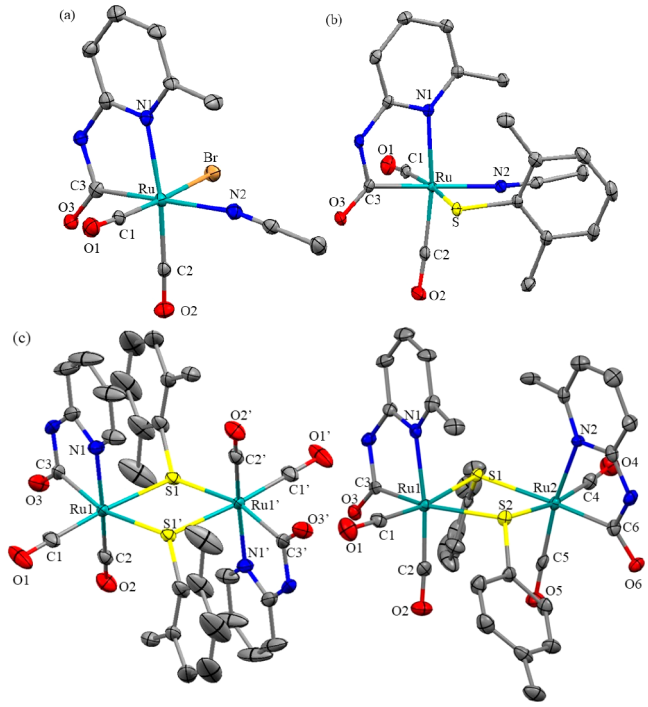

Figure 2. ORTEP plots showing the molecular structures of (a) **2b**, (b) **3bB**, and (c) **4aB** (left) and **4bA** (right). Thermal ellipsoids are drawn at the 50% probability level, and all hydrogen atoms were omitted for clarity.

Isomerism. Steric effects of the 6-substituent on the pyridine ring are apparent in the bond parameters of **2a** and **2b**. These include an increasing angle between the pyridine ring and the acetonitrile and a longer Ru–N1 bond in moving from R = H (**2a**) to Me (**2b**); ∠N1–Ru–N2 = 92.73(8)° and 101.6(1)°, and d(Ru–N1) = 2.110(2) and 2.163(3) Å, respectively. There is also greater distortion of the five-membered metallacycle, which does not lie directly above the Ru–N2 bond, in **2b**; the N(2)–Ru–N(1)–R torsion angles are −2.43° and −11.40° in **2a** and **2b**, respectively. One chemical consequence of this steric interaction is that **2b** is present as one isomer in solution, while **2a** exists as a mixture of two isomers; the IR spectrum of **2b** shows only two bands for the CO stretches, while that for **2a** shows a split in the lower frequency band (*vide infra*). Similarly, the ^{1}H NMR spectrum of **2a** shows two sets of resonances, in a 55:45 ratio, but only one for **2b**. The observation of two isomers in **2a** is also in agreement with an earlier report on an iron analogue.[14d] A series of VT ^{1}H NMR spectra of **2a** shows broadening and coalescence at higher temperatures, indicating isomerization at the NMR time scale (Figure 3).

The exchange rate and activation energy barrier estimated from the coalescence of the doublet at ∼8.35 ppm are 12 s^{-1} and 75 kJ mol^{-1}, respectively, at the coalescence temperature of 70 °C. In contrast, the VT ^{1}H NMR spectra of **2b** show no significant broadening of the resonances, except for the NH resonance (Figure S9), consistent with the presence of essentially one isomer.

A computational study carried out on all seven possible stereoisomers of **2a** and **2b** (Tables S6 and S7) shows that the energy gap between the two lowest energy isomers (Figure 3 and Table S8) is about 1 and 8 kJ mol^{-1}, which corresponds to an isomeric ratio of 60:40 and 96:4 for **2a** and **2b**, respectively.

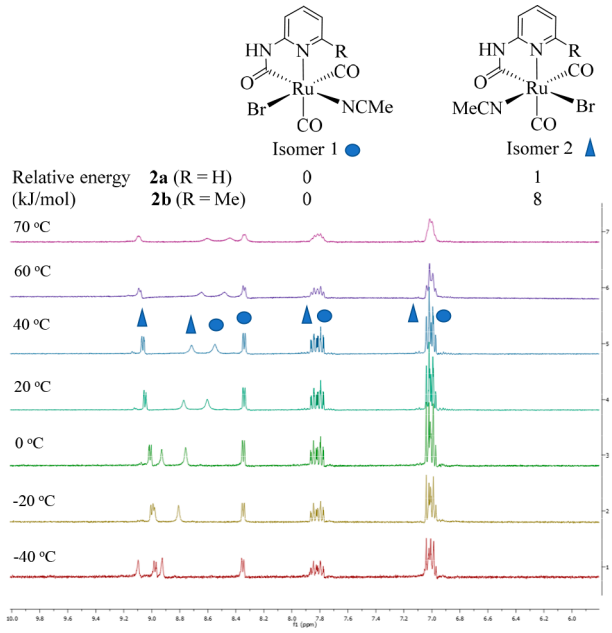

Figure 3. Top: Computed free energies (in kJ/mol) of the two lowest energy isomers of **2a** and **2b** relative to the most stable isomer (isomer 1). Bottom: VT ^{1}H NMR spectra of **2a** in d_3-acetonitrile.

These values are in very good agreement with those from NMR integration. The computed values for the CO vibrations also point to a larger difference (~10 cm^{-1}) in the lower frequency band between the isomers (Table S6), in agreement with the observed splitting of this band. The major isomer for both **2a** and **2b** from the computational study (isomer 1) corresponds to that observed in the solid-state structure; thus, the minor isomer in **2a** is presumably isomer 2. The relative stability of the isomers can be rationalized on the basis of the *trans* influence: NHCO > CO > Br^- > MeCN > Py.[20] Thus, the strongly π-accepting CO and the strongly σ-donating carbamoyl prefer to be *trans* to weak π-acceptors or−donors such as Br^-, MeCN, or Py. The larger isomer energy gap in **2b** may be attributed to steric interaction between the bulky bromide ligand and the methyl substituent of the pyridine ring.

Dissolution in Polar Solvents. Complex **3bB** is a ruthenium-based structural mimic of the [Fe]-hydrogenase active site, with acetonitrile in place of the unknown sixth ligand.[14d] The infrared spectrum (in acetonitrile) shows two intense absorption bands at 2047 and 1978 cm^{-1} ($\Delta\nu$ = 69 cm^{-1}) for the *cis*-dicarbonyl ligands which are blue-shifted from that for the previously reported iron analogues (~20 cm^{-1})[14d] and the [Fe]-hydrogenase (~15 cm^{-1}),[11] consistent with ruthenium being less electron-rich.[21,22]

Although complexes **2** and **3** are not very soluble in most of the common organic solvents, their solubility in acetone and tetrahydrofuran increased upon the addition of small amounts of water. It is also noted that the CO vibrations of **2b** in acetone, for example, are blue-shifted with increasing amounts of water added (Figure S4), and a similar shift is observed for **3bB** in acetonitrile (Figure S5). These shifts are indicative of changes in composition, and in the case of **2b** in acetonitrile, may be attributed to the formation of a new species upon the addition of water, which has tentatively been identified as a cationic species in which both the Br^- and MeCN ligands have been replaced by water molecules; the experimental ν_{CO} values at 2086 and 2027 cm^{-1} are in good agreement with the values of 2089 and 2028 cm^{-1} calculated for this species (Figure 4).

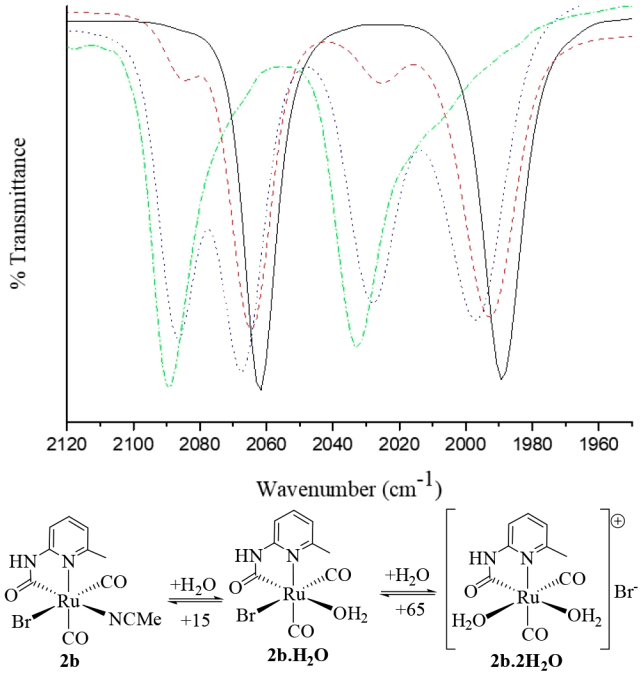

Compounds	**2b**	**2b.H_2O**	**2b.2H_2O**
Experimental ν_{CO} (cm^{-1})	2062, 1989	-	2086, 2027
Computed ν_{CO} (cm^{-1})	2057, 1981	2055, 1984	2089, 2028

Figure 4. (Top) IR spectra of **2b** in acetonitrile (black solid line) and various compositions of acetonitrile/water (v/v): 10:1 (red dashed line), 5:2 (purple dashed line), and 1:2 (green dashed-dot line). (Bottom) Proposed exchange process. Free energies are given in kJ/mol for the forward reactions.

Computational studies on both **2b** and **3bB** also suggest that replacement of the acetonitrile ligand with water will lead to a decrease in the frequency difference between the two CO vibrational modes, as observed in the experimental spectra (Table S5). The weak Ru−OH_2 bond is corroborated by the mass spectrum; the molecular ion peak for **2b** can be observed at ambient temperature but not at higher temperatures. The resonance at 2.10 ppm for the metal-bound CH_3CN ligand in the ^{1}H NMR spectrum (in acetone-d_6) shifts to 2.05 ppm, corresponding to free acetonitrile, upon addition of water (Figure S12).[23] A density functional theory (DFT) calculation gives a $\Delta G°$ of −0.1 kJ mol^{-1} for the reaction: **2b** + H_2O → **2b**·H_2O + CH_3CN (in acetone). All of these indicate that the sixth (acetonitrile) ligand in **2** and **3** is very weakly bound, reminiscent of the situation in the [Fe]-hydrogenase.[8,10]

Bioconjugation to Papain. That complexes **2** can be thiolated suggests that they may also be incorporated into a protein via reaction with a free sulfhydryl moiety. Papain contains a free sulfhydryl moiety borne by Cys25 which, together with His159, are the two essential amino acids responsible for its proteolytic activity.[19] Conjugation to the sulfhydryl group of Cys25 can thus be readily monitored via a

fall in its enzymatic activity. As histidine residues such as His159 may also be involved in coordination owing to their imidazole group, a preliminary assessment of the reactivity of **2b** with imidazole was first carried out.

We found that **2b** reacts with imidazole to give **2b·Im**, and this can in turn react with *N*-acetyl-L-cysteine-methyl ester (**C**) to afford the dimer **4bC**; the latter can also be obtained directly from the reaction of **2b** and **C** (Scheme 3). The

Scheme 3. Reaction of 2b and 3bB with Imidazole and *N*-Acetyl-L-cysteine-methyl Ester

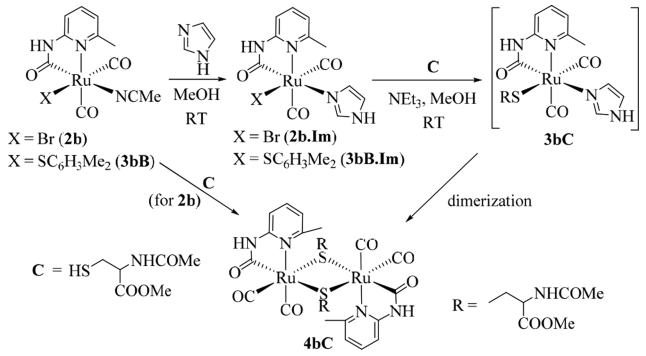

complex **3bB** reacts similarly with imidazole to form **3bB·Im**. Both the imidazole complexes **2b·Im** and **3bB·Im**, however, slowly convert back to **2b** and **3bB**, respectively, on standing in acetonitrile (Figures S7 and S8). These results suggest that conjugation of **2b** to a cysteine side chain should be favored over histidine.

Conjugation of **2b** to papain was assessed through measurement of its effect on the hydrolysis rate of *N*-α-carbobenzoxy-glycine *p*-nitrophenyl ester (ZGlyONP).[24] The activity dropped to almost zero, suggesting that Cys25 was affected (Figure S16). After a gel filtration step to remove excess complex, bioconjugate **5** was analyzed by several spectroscopic techniques. The UV−visible spectrum of **5** (Figure S17) shows two peaks at 279 and ∼318 nm ascribable to papain[25] and the ruthenium center, respectively. The IR spectrum of **5** shows that the characteristic carbonyl bands are red-shifted (2064 and 2000 cm^{-1}) from that of **2b** (Figure 5). This red shift is similar to the shift in comparing **2b** with **3bB**, and the smaller frequency gap between the two stretches (64 cm^{-1}) is also consistent with thiolation. Indeed, the frequency gap is the same as that computed for **3bB**·H_2O (corresponding

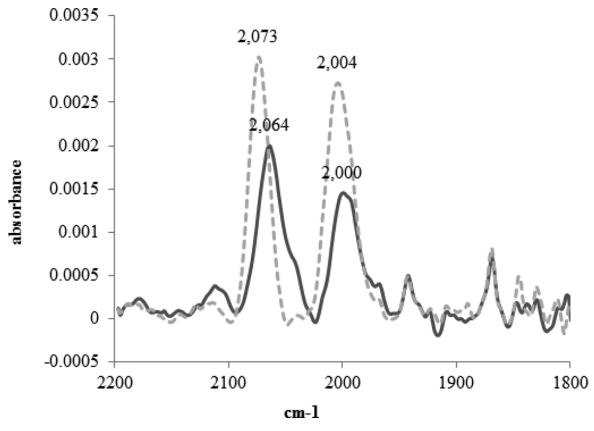

Figure 5. IR spectra of **2b** (gray dotted line) and **5** (black full line).

to replacement of the acetonitrile ligand in **3bB** with water), suggesting that **5** contains thiolato and water ligands (Table S5).

While the electrospray ionization-high resolution mass spectrum (ESI-HRMS) of papain reveals a charge states distribution from 22+ (*m*/*z* 1065.69) to 12+ (*m*/*z* 1952.82), centered around 18+ (*m*/*z* 1302.28) and 17+ (*m*/*z* 1378.82) (Figure 6A), that for **5** shows charge states ranging from 22+

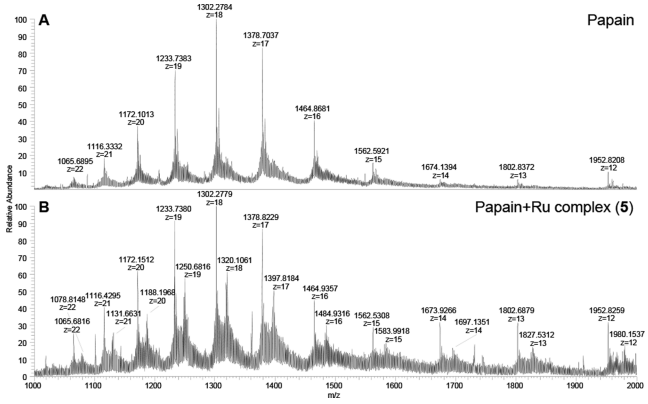

Figure 6. ESI-HRMS mass spectra of (A) papain and (B) bioconjugate **5**, both at 2.15 μM in water/acetonitrile/formic acid (49:50:1, v/v/v).

(*m*/*z* 1078.81) to 12+ (*m*/*z* 1980.15) (Figure 6B). After deconvolution and deisotoping, the mass spectrum of papain showed a major peak at a monoisotopic mass of 23 407.52205, in good agreement with the theoretical value (23 407.52457 g·mol^{-1}; 0.2 ppm) (Figure S15A). Another species at a mass of 23 437.52205, corresponding to an amino acid variant with Thr in place of an Ala residue (mass shift of +30.01056) was also observed. In comparison, that for **5** showed two prominent additional species at 23 699.47624 and 23 729.48682, corresponding to an exact mass shift of 291.95417 (Figure S15B). This value matches very well with the conjugation of **2b** to papain by substitution of the bromide ligand by a thiolate (and loss of MeCN). Interestingly, no other species at higher mass was observed, indicating monometalation of the protein.

3. CONCLUSION

In this study, we showed that organoruthenium complexes of the general formula [Ru(2-NHC(O)C_5H_3NR)$(CO)_2$(X)(L)] (where R = H, Me, X = Br or SR′, and L = H_2O or $NCCH_3$) exhibited chemistry that is relevant to understanding the chemistry of the [Fe]-hydrogenase: the lability of the so-called sixth ligand and the importance of steric bulk in preventing dimerization via thiolate bridges through this coordination site. We believe that embedding of the metal cofactor in a protein cavity is how nature achieves this and showed that this can be readily achieved with the complexes reported here. The extension of this idea to the construction of metalloenzymes is ongoing.

4. EXPERIMENTAL SECTION

General Procedures. All experiments were performed under an argon atmosphere using standard Schlenk techniques except for the bioconjugation experiments. Chemicals were obtained from Sigma-Aldrich and used as received. Papain was obtained from Calbiochem.[24,26] Compounds **1** were synthesized as previously

described.[16] Solvents used for reactions were distilled over the appropriate drying agents under argon before use. ESI-HRMS for compounds were recorded on a Waters UPLC-Q-Tof MS mass spectrometer, while that for papain and bioconjugate **5** were performed on a LTQ-Orbitrap XL. ^{1}H and ^{13}C{^{1}H} NMR spectra were obtained on a JEOL 400 MHz spectrometer at room temperature unless stated otherwise. Chemical shifts for ^{1}H and ^{13}C{^{1}H} were referenced with respect to the residual resonances of the respective deuterated solvents. Infrared spectra were recorded on a Bruker Alpha FT-IR spectrometer in an IR cell with NaCl windows and a path length of 0.1 mm at a resolution of 2 cm^{-1}; for the bioconjugation experiments, the spectra were recorded after deposition of the solutions onto nitrocellulose membrane and air-dried. Absorbance spectra were recorded using a Varian Cary 50 spectrometer. Elemental analyses were performed on a PerkinElmer 2400 Series II CHN/O Elemental Analyzer in house.

*Preparation of [RuBr(2-NHC(O)C$_5$H$_4$N)(CO)$_2$(NCMe)] (**2a**).* A sample of **1a** (200 mg, 0.38 mmol) was dissolved in acetonitrile (50 mL). Slow evaporation of the solvent at room temperature afforded white crystal of **2a**. Yield: 100 mg, 0.26 mmol, 68%. mp 343−344 °C. IR (acetonitrile, cm^{-1}): ν_{CO} 2061 (vs), 1999 (s), 1989 (s), 1622 (m). ^{1}H NMR (CD$_3$CN): δ 9.10−9.09 (d, 1H, J = 5.5 Hz, PyH), 8.71−8.69 (br, 1H, NH), 8.54−8.552 (br, 1H, NH), 8.37−8.36 (d, 1H, J = 5.5 Hz, PyH), 7.89−7.80 (m, 2H, PyH), 7.06−7.00 (m, 4H, PyH), 1.96 (s, 6H, Me) ppm. ^{13}C{^{1}H} NMR (CD$_3$CN): 198.8 (CO), 198.2 (CO), 195.8 (CO), 195.6 (CO), 195.4 (NHCO), 191.2 (NHCO), 158.0, 157.5, 148.6, 147.5, 141.2, 140.6, 116.8, 116.5, 109.3, 109.5 ppm. HRMS. Calcd for [M]$^+$: m/z: 399.8871. Found: m/z 399.8876. Anal. Calcd for C$_8$H$_5$N$_2$O$_3$BrRu (M-CH$_3$CN): C 26.83, H 1.41, N 7.82. Found C 26.90, H 1.86, N 7.21.

Complex **2b** was similarly prepared from **1b** (213 mg, 0.38 mmol). Yield: 113 mg, 0.27 mmol, 72%. mp 281−282 °C. IR (acetonitrile, cm^{-1}): ν_{CO} 2061 (vs), 1988 (s), 1619 (m). ^{1}H NMR (CD$_3$CN): δ 8.52−8.50 (br, 1H, NH), 7.67−7.63 (t, 1H, J = 7.8 Hz, PyH), 6.88−6.86 (t, 1H, J = 7.8 Hz, PyH), 6.82−6.80 (d, 1H, J = 8.2 Hz, PyH), 2.65 (s, 3H, Me), 1.98 (s, 3H, Me) ppm. ^{13}C{^{1}H} NMR ((CD$_3$)$_2$CO): 195.1 (CO), 191.8 (CO), 159.5 (NHCO), 158.4, 140.2, 117.2, 116.6, 106.9, 25.5 ppm. HRMS. Calcd for [M + H]$^+$: m/z: 413.9027. Found: m/z 413.9021. Anal. Calcd for C$_{11}$H$_{10}$N$_3$O$_3$BrRu: C 31.98, H 2.44, N 10.17. Found C 31.70, H 2.40, N 10.48.

*Preparation of [Ru(2-NHC(O)C$_5$H$_3$NMe)(SC$_6$H$_3$Me$_2$)(CO)$_2$(NCMe)] (**3bB**).* Triethylamine (7 μL, 0.05 mmol) and 2,6-dimethylbenzenethiol (5 μL, 0.05 mmol) were added into a solution of **2b** (21 mg, 0.05 mmol) in acetonitrile (5 mL). The resulting solution was then stirred for 5 min at room temperature. Slow evaporation of the solvent at room temperature afforded **3bb** as yellow crystals. Yield: 13 mg, 0.03 mmol, 55%. IR (MeCN, cm^{-1}): ν_{CO} 2047 (vs), 1978 (s). ^{1}H NMR (CD$_3$CN): δ 8.45 (br, 1H, NH), 7.64−7.60 (t, 1H, J = 7.4 Hz, PyH), 6.92−6.90 (d, 2H, J = 7.8 Hz, PyH), 6.83−6.75 (m, 3H, PyH), 2.44 (s, 3H, Me), 2.24 (s, 6H, Me), 1.96 (s, 3H, Me) ppm. ^{13}C{^{1}H} NMR (CD$_3$CN): 159.5, 143.4, 139.6, 129.9, 123.3, 126.3, 123.5, 116.4, 106.4, 22.2, 20.9 ppm. HRMS. Calcd for [M + H]$^+$: m/z: 472.0520. Found: m/z 472.0539. Anal. Calcd for C$_{19}$H$_{19}$N$_3$O$_3$SRu: C 48.50, H 4.07, N 8.93, S 6.81. Found C 48.47, H 4.46, N 9.21, S 6.73.

*Preparation of [Ru(2-NHC(O)C$_5$H$_4$N)(SC$_6$H$_4$Me)(CO)$_2$]$_2$ (**4aA**).* Triethylamine (5 μL, 0.05 mmol) and 4-methylbenzenethiol (6 mg, 0.05 mmol) were added into a solution of **2a** (20 mg, 0.05 mmol) in acetonitrile (5 mL) at room temperature. A white precipitate was formed immediately, and the solution was left to stir for 2 h. The white precipitate was separated by filtration and washed with acetonitrile (20 mL) to afford analytically pure **4aA**. Yield: 25 mg, 0.03 mmol, 60%. IR (MeCN, cm^{-1}): ν_{CO} 2053 (m), 2037 (s), 1991 (m), 1970 (s). ^{1}H NMR ((CD$_3$)$_2$SO): δ 10.70 (br, 1H, NH), 8.35−8.34 (d, 1H, J = 5.04 Hz, PyH), 8.00−7.95 (m, 1H, PyH), 7.47−7.45 (d, 2H, J = 8.72 Hz, PhH), 7.16−7.14 (d, 1H, J = 8.24 Hz, PyH), 7.05−7.03 (d, 2H, J = 5.04 Hz, PhH), 6.93−6.89 (m, 1H, J = 5.04 Hz, PyH), 2.25 (s, 3H, Me) ppm. ^{13}C{^{1}H} NMR ((CD$_3$)$_2$SO): 201.9, 201.4, 193.2, 158.5, 148.1, 141.3, 135.2, 134.6, 132.3, 129.5, 118.6, 110.5, 21.0 ppm. HRMS. Calcd for [M + H]$^+$: m/z: 804.9312. Found: m/z 804.9329.

Complexes **4aB** and **4bA** were prepared in similar yields following an analogous procedure.

4aB. IR (KBr, cm^{-1}): ν_{CO} 2041 (s), 1979 (s). HRMS. Calcd for [M + H]$^+$: m/z: 832.9625. Found: m/z 832.9624. MS. Calcd for [M + Na]$^+$: m/z: 853.7. Found: m/z 853.8. Anal. Calcd for C$_{32}$H$_{28}$N$_4$O$_6$S$_2$Ru$_2$: C 46.26, H 3.40, N 6.74, S 7.72. Found C 46.33, H 3.33, N 6.98, S 7.72.

4bA. IR (KBr, cm^{-1}): ν_{CO} 2051 (m), 2038 (s), 1988 (m), 1975 (s). ^{1}H NMR (d_6-DMSO): δ 10.50 (br, 1H, NH), 7.80−7.77 (t, 1H, J = 8.2 Hz, PyH), 7.52−7.51 (d, 2H, J = 8.2 Hz, PhH), 7.03−7.01 (d, 2H, J = 7.8 Hz, PhH), 6.90−6.91 (d, 1H, J = 4.9 Hz, PyH), 6.82−6.80 (d, 1H, J = 8.2 Hz, PyH), 2.49 (s, 3H, Me), 2.24 (s, 3H, Me) ppm. ^{13}C{^{1}H} NMR (d_6-DMSO): 202.3, 199.7, 194.1, 160.7, 159.4, 141.1, 136.8, 134.4, 131.4, 129.5, 118.6, 108.1, 28.3, 20.9 ppm. HRMS. Calcd for [M + H]$^+$: m/z: 832.9625. Found: m/z 832.9626.

*Preparation of [RuBr(2-NHC(O)C$_5$H$_3$NMe)(CO)$_2$(C$_3$H$_4$N$_2$)] (**2b·Im**).* A sample of imidazole (1.6 mg, 0.02 mmol) was added into a solution of **2b** (10 mg, 0.02 mmol) in methanol (5 mL). The resulting mixture was then stirred for 30 min at ambient temperature. Slow evaporation of the solvent afforded **2b·Im** as a crystalline solid. Yield: 3 mg, 0.01 mmol, 34%). IR (MeOH, cm^{-1}): 2062 (s), 1998 (s). ^{1}H NMR (d_6-acetone): δ 11.95 (br, 1H, NH), 9.66 (br, 1H, NH), 8.24 (s, 1H, CH), 7.71−7.67 (t, 1H, J = 7.8 Hz, PyH), 7.25−7.20 (d, 2H, J = 10.5 Hz, CH), 6.93−6.87 (m, 2H, PyH), 3.06 (s, 3H, Me) ppm. ^{13}C{^{1}H} NMR (d_6-acetone): 202.2, 197.4, 196.1, 162.0, 158.9, 140.4, 139.4, 129.0, 117.7, 117.0, 106.6, 25.0 ppm. HRMS. Calcd for [M + H]$^+$: m/z: 440.0828. Found: m/z 440.0812. Anal. Found C 34.37, H 2.80, N 13.59; Calculated for C$_{12}$H$_{11}$N$_4$O$_3$BrRu.C$_2$H$_3$N: C 34.94, H 2.93, N 14.55.

*Preparation of [Ru(2-NHC(O)C$_5$H$_3$NMe)(SCH$_2$CH(NHCOMe)-CO$_2$Me)(CO)$_2$]$_2$ (**4bC**).* Triethylamine (3 μL, 0.02 mmol) and *N*-acetyl-L-cysteine-methyl ester (4.3 mg, 0.02 mmol) were added into a solution of **2b** (10 mg, 0.02 mmol) in methanol (5 mL). The resulting mixture was stirred for 30 min, and then the volume was reduced under vacuum to approximately 1 mL. After standing for 3 d, complex **4bC** (9.0 mg, 0.01 mmol, 48%) was obtained as a yellow crystalline solid. IR (MeOH, cm^{-1}): 2052 (s), 2038 (s), 1991 (s), 1978(s). ^{1}H NMR (d_3-acetonitrile): δ 8.90 (br, 1H, NH), 7.71−7.66 (m, 1H, PyH), 6.90−6.86 (m, 1H, PyH), 6.73−6.68 (m, 1H, PyH), 4.44−4.39 (m, 1H, CH), 3.59 (s, 3H, Me), 3.27−3.18 (m, 2H, CH2), 2.16 (s, 3H, Me), 1.88 (s, 3H, Me) ppm. HRMS. Calculated for [M + H]$^+$: m/z: 938.9851 Found: m/z 938.9877.

Purification of Papain by Affinity Chromatography.[27] The peptide GGYR (Bachem) was attached to CNBr-activated Sepharose 4B (Sigma) via its terminal NH$_2$ group. The resin (20 mL) was packed into a column (XK 16, GE Healthcare) and conditioned with EDTA (20 mM) and mercaptoethanol (10 mM) pH 4.3, at 1 mL/min. Papain (200 mg solid, Calbiochem) was dissolved in EDTA (25 mM), mercaptoethanol (30 mM) pH 4.3 (20 mL), and the solution was incubated for 30 min. The solution (18 mL) was injected into the column, and the resin was washed successively with conditioning buffer (2 volumes) then with washing buffer (5 mM EDTA, pH 6.0, 2 volumes). Papain was finally eluted with water (2 volumes). Protein concentration was calculated from the absorbance at 280 nm taking an extinction coefficient of 56 000 M^{-1}·cm^{-1}.

Enzymatic Assay. Affinity-purified papain (1.6 mL of a 3.2 μM solution in water; final concentration = 2.56 μM) was mixed with 50 mM phosphate buffer pH 7.8 and **2b** (20 μL of a 10 mM solution; final concentration = 100 μM). Twenty microliters of the mixture was used to measure the hydrolytic activity of ZGlyONP (50 μL) in 430 μL of phosphate buffer pH 6.5 at various times. The remaining mixture was incubated at RT for 18 h and submitted to gel filtration on a dextran desalting column (10 mL, Thermo scientific). Species were eluted with water. One milliliter fractions were collected, and their absorbance at 280 nm was measured with a spectrophotometer. The fractions containing the protein were pooled, and the solution (3 mL; 1.25 μM) was concentrated by ultrafiltration on Amicon Ultra 4 (10 kDa cutoff, Millipore) to a final volume of 0.22 mL. A control

experiment using papain was also carried out to measure the hydrolytic activity of ZGlyONP.

High Resolution Mass Spectrometry of Papain Samples. ESI-HRMS experiments were carried out using a LTQ-Orbitrap XL from Thermo Scientific (San Jose, CA, United States) and operated in positive ionization mode, with a spray voltage at 4.5 kV. Native papain or bioconjugate **5** in a water/acetonitrile/formic acid (49:50:1, v/v/v) mixture was continuously infused using a 250 μL syringe at 5 μL/min flow. Applied voltages were 40 and 100 V for the ion transfer capillary and the tube lens, respectively. The ion transfer capillary was held at 275 °C. Sheath and auxiliary gas were set at a flow rate of 45 and 15 arbitrary units (a.u.), respectively. Detection was achieved in the Orbitrap with a resolution set to 100 000 (at m/z 400) and a m/z range between 200 and 3000 in profile mode. Spectrum was analyzed using the acquisition software XCalibur 2.1 (Thermo Fisher Scientific, Courtaboeuf, France) without smoothing and background subtraction. The automatic gain control (AGC) allowed accumulation of up to 2×10^5 ions for FTMS scans. Maximum injection time was set to 500 ms, and 1 μscan was acquired.

Crystallographic Studies. Diffraction-quality crystals were grown from acetonitrile (**2a**, **2b**, **3bB**, **4aA**, **4aB**, and **4bA**) mounted on quartz fibers. X-ray diffraction data were collected at 103(2) K on a Bruker X8 APEX system, using Mo Kα radiation, with the SMART suite of programs.[28] Data processing and correction were made for Lorentz and polarization effects with SAINT,[29] and adsorption effects with SADABS.[30] Twinning was observed for the crystals of **4bA**; the twin laws and cell parameters were determined using the program CELL_NOW,[31] and the reflection data processed and corrections applied using the program TWINABS.[32] Structural solution and refinement were carried out with the SHELXTL suite of programs.[33] The structures were solved by direct methods to locate the heavy atoms, followed by successive difference maps for the light, nonhydrogen atoms. Disorder of a carbonyl and the bromide ligand was found for **2b**, which were modeled with two sites each, with occupancies summed to unity. All nonhydrogen atoms were refined with anisotropic displacement parameters in the final model. All organic hydrogen atoms were placed in calculated positions and refined with a riding model. The crystallographic data are summarized in Tables S1 and S2.

Computational Studies. The computational studies were carried out using DFT, utilizing the hybrid functional of Truhlar and Zhao (M06).[34] The basis set used was def2TZVP for ruthenium[35] and 6-311+G(2d,p) for the light atoms. For calculations involving solvated species, the polarized continuum model was employed. Spin-restricted calculations were used for structural optimization, harmonic frequency calculations and to evaluate zero-point energy corrections. Optimized geometries were characterized as equilibrium structures with all real frequencies. All calculations were performed using the Gaussian 09 suite of programs.[36] The coordinates for parent complexes were taken from the crystal structure, and each of the other isomers was modified from this.

■ ASSOCIATED CONTENT

Supporting Information

The Supporting Information is available free of charge on the ACS Publications website at DOI: 10.1021/acs.inorgchem.8b01835.

NMR spectra showing presence of isomers, crystallographic tables, and optimized geometry of computed structures, experimental procedure and high-resolution mass spectra of papain and bioconjugate (PDF)

Accession Codes

CCDC 1820446, 1820447, 1839988, 1839990, 1839991, and 1839992 contain the supplementary crystallographic data for this paper. These data can be obtained free of charge via www.ccdc.cam.ac.uk/data_request/cif, y emailing data_request@ccdc.cam.ac.uk, or by contacting The Cambridge Crystallographic Data Centre, 12 Union Road, Cambridge CB2 1EZ, UK; fax: +44 1223 336033.

■ AUTHOR INFORMATION

Corresponding Authors

*E-mail: chmlwk@ntu.edu.sg.

*E-mail:Michele.salmain@sorbonne-universite.fr.

ORCID

Cédric Przybylski: 0000-0003-0352-1461

Michèle Salmain: 0000-0003-3039-5659

Weng Kee Leong: 0000-0003-3198-7111

Notes

The authors declare no competing financial interest.

■ ACKNOWLEDGMENTS

This work was supported by the Nanyang Technological University and a research grant from the Agency for Science, Technology and Research (A*STAR) (Research Grant M4070244). C.K.B is grateful to the university for the Research Scholarships.

■ REFERENCES

(1) Stephenson, M.; Stickland, L. H. Hydrogenase: A Bacterial Enzyme Activating Molecular Hydrogen. *Biochem. J.* **1931**, *25*, 205−214.

(2) Vignais, P. M.; Billoud, B.; Meyer, J. Classification and Phylogeny of Hydrogenases. *FEMS Microbiol. Rev.* **2001**, *25*, 455−501.

(3) Frey, M. Hydrogenases: Hydrogen-Activating Enzymes. *ChemBioChem* **2002**, *3*, 153−160.

(4) Thauer, R. K.; Klein, A. R.; Hartmann, G. C. Reactions with Molecular Hydrogen in Microorganisms: Evidence for a Purely Organic Hydrogenation Catalyst. *Chem. Rev.* **1996**, *96*, 3031−3042.

(5) Corr, M. J.; Roydhouse, M. D.; Gibson, K. F.; Zhou, S.-Z.; Kennedy, A. R.; Murphy, J. A. Amidine Dications as Superelectrofiles. *J. Am. Chem. Soc.* **2009**, *131*, 17980−17985.

(6) Kalz, K. F.; Brinkmeier, A.; Dechert, S.; Mata, R. A.; Meyer, F. Functional Model for the [Fe]-Hydrogenase Inspired by the Frustrated Lewis Pair Concept. *J. Am. Chem. Soc.* **2014**, *136*, 16626−16634.

(7) Lyon, E. J.; Shima, S.; Boecher, R.; Thauer, R. K.; Grevels, F.-W.; Bill, E.; Roseboom, W.; Albracht, S. P. Carbon Monoxide as an Intrinsic Ligand to Iron in the Active Site of the Iron-Sulfur-Cluster-free Hydrogenase H_2-Forming Methylenetetrahydromethanopterin Dehydrogenase as Revealed by Infrared Spectroscopy. *J. Am. Chem. Soc.* **2004**, *126*, 14239−14248.

(8) Shima, S.; Pilak, O.; Vogt, S.; Schick, M.; Stagni, M. S.; Meyer-Klaucke, W.; Warkentin, E.; Thauer, R. K.; Ermler, U. The Crystal Structure of [Fe]-Hydrogenase Reveals the Geometry of the Active Site. *Science* **2008**, *321*, 572−575.

(9) Shima, S.; Lyon, E. J.; Thauer, R. K.; Mienert, B.; Bill, E. Mossbauer Studies of the Iron-Sulfur Cluster-free Hydrogenase: The Electronic State of the Mononuclear Fe Active Site. *J. Am. Chem. Soc.* **2005**, *127*, 10430−10435.

(10) Tard, C.; Pickett, C. J. Structural and Functional Analogues of the Active Sites of the [Fe]-[NiFe]-, and [FeFe]-Hydrogenases. *Chem. Rev.* **2009**, *109*, 2245−2274.

(11) Hiromoto, T.; Ataka, K.; Pilak, O.; Vogt, S.; Stagni, M. S.; Meyer-Klaucke, W.; Warkentin, E.; Thauer, R. K.; Shima, S.; Ermler, U. The Crystal Structure of C176A Mutated [Fe]-Hydrogenase Suggests an Acyl-Iron Ligation in the Active Site Iron Complex. *FEBS Lett.* **2009**, *583*, 585−590.

(12) Shima, S.; Thauer, R. K. A Third Type of Hydrogenase Catalyzing H_2 Activation. *Chem. Rec.* **2007**, *7*, 37−46.

(13) Lyon, E. J.; Shima, S.; Buurman, G.; Chowdhuri, S.; Batschauer, A.; Steinbach, K.; Thauer, R. K. UV-A/blue-light Inactivation of the

'Metal-free' Hydrogenase (Hmd) from Methanogenic Archaea. *Eur. J. Biochem.* **2004**, *271*, 195−204.

(14) (a) Royer, A. M.; Rauchfuss, T. B.; Gray, D. L. Oxidative Addition of Thioesters to Iron(0): Active-Site Models for Hmd, Nature's Third Hydrogenase. *Organometallics* **2009**, *28*, 3618−3620. (b) Chen, D.; Scopelliti, R.; Hu, X. Synthesis and Reactivity of Iron Acyl Complexes Modeling the Active Site of [Fe]-Hydrogenase. *J. Am. Chem. Soc.* **2010**, *132*, 928−929. (c) Chen, D.; Scopelliti, R.; Hu, X. [Fe]-Hydrogenase Models Featuring Acylmethylpyridinyl Ligands. *Angew. Chem., Int. Ed.* **2010**, *49*, 7512−7515. (d) Turrell, P. J.; Wright, J. A.; Peck, J. N.; Oganesyan, V. S.; Pickett, C. J. The Third Hydrogenase: A Ferracyclic Carbamoyl with Close Structural Analogy to the Active Site of Hmd. *Angew. Chem., Int. Ed.* **2010**, *49*, 7508−7511. (e) Wright, J. A.; Turrell, P. J.; Pickett, C. J. The Third Hydrogenase: More Natural Organometallics. *Organometallics* **2010**, *29*, 6146−6156. (f) Chen, D.; Ahrens-Botzong, A.; Schünemann, V.; Scopelliti, R.; Hu, X. Synthesis and Characterization of a Series of Model Complexes of the Active Site of [Fe]-Hydrogenase (Hmd). *Inorg. Chem.* **2011**, *50*, 5249−5257. (g) Turrell, P. J.; Hill, A. D.; Ibrahim, S. K.; Wright, J. A.; Pickett, C. J. Ferracyclic Carbamoyl Complexes Related to the Active Site of [Fe]-Hydrogenase. *Dalton Trans* **2013**, *42*, 8140−8146. (h) Song, L.-C.; Hu, F.-Q.; Wang, M.-M.; Xie, Z.-J.; Xu, K.-K.; Song, H.-B. Synthesis, Structural Characterization, and Some Properties of 2-acylmethyl-6-ester Group-difunctionalized Pyridine-containing Iron Complexes Related to the Active Site of the [Fe]-Hydrogenase. *Dalton Trans* **2014**, *43*, 8062−8071. (i) Xu, T.; Yin, C.-J. M.; Wodrich, M. D.; Mazza, S.; Schultz, K. M.; Scopelliti, R.; Hu, X. A Functional Model of [Fe]-Hydrogenase. *J. Am. Chem. Soc.* **2016**, *138*, 3270−3273. (j) Song, L.-C.; Xu, K.-K.; Han, X.-F.; Zhang, J.-W. Synthesis and Structural Studies of 2-Acylmethyl-6-Difunctionalized Pyride Ligand-Containing Iron Complexes Related to [Fe]-Hydrogenase. *Inorg. Chem.* **2016**, *55*, 1258−1269. (k) Xie, Z.-L.; Durgaprasad, G.; Ali, A. K.; Rose, M. J. Substitution Reactions of Iron(II) Carbamoyl-thioether Complexes Related to Mono-iron Hydrogenase. *Dalton Trans* **2017**, *46*, 10814−10829. (l) Song, L.-C.; Zhu, L.; Hu, F.-Q.; Wang, Y.-X. Studies on Chemical Reactivity and Electrocatalysis of Two Acylmethyl-(hydroxymethyl)pyridine Ligand-Containing [Fe]-Hydrogenase Models (2-$COCH_2$-6-$HOCH_2C_5H_3N$)$Fe(CO)_2L$ (L = η^1-SCOMe, η^1-2-SC_5H_4N). *Inorg. Chem.* **2017**, *56*, 15216−15230. (m) Seo, J.; Manes, T. A.; Rose, M. J. Structural and Functional Synthetic Model of Mono-Iron Hydrogenase featuring an Anthracene Scaffold. *Nat. Chem.* **2017**, *9*, 552−557. (n) Kerns, S. A.; Magtaan, A.-C.; Vong, P. R.; Rose, M. J. Functional Hydride Transfer by a Thiolate-Containing Model of Mono-Iron Hydrogenase featuring an Anthracene Scaffold. *Angew. Chem., Int. Ed.* **2018**, *57*, 2855−2858.

(15) Shima, S.; Chen, D.; Xu, T.; Wodrich, M. D.; Fujishiro, T.; Schultz, K. M.; Kahnt, J.; Ataka, K.; Hu, X. Reconstitution of [Fe]-Hydrogenase using Model Complexes. *Nat. Chem.* **2015**, *7*, 995−1002.

(16) Barik, C. K.; Ganguly, R.; Li, Y.; Leong, W. K. Structural Mimics of the [Fe]-Hydrogenase: A Complete Set for Group VIII Metals. *Inorg. Chem.* **2018**, *57*, 7113−7120.

(17) Rohmann, K.; Kothe, J.; Haenel, M. W.; Englert, U.; Hölscher, M.; Leitner, W. Hydrogenation of CO_2 to Formic Acid with a Highly Active Ruthenium Acriphos Complex in DMSO and DMSO/Water. *Angew. Chem., Int. Ed.* **2016**, *55*, 8966−8969.

(18) Chen, M.-H.; Lin, J.-H.; Li, C.-R.; Gliniak, J.; Chang, C.-H.; Peng, C.-S.; Chen, Y.-T.; Yu, J.-S. K.; Wu, T.-K. Enhanced hydrogen generation from formic acid by a biomimetic ruthenium complex with a covalently bonded phosphine ligand. *Int. J. Hydrogen Energy* **2017**, *42*, 9784−9794.

(19) Chevalley, A.; Cherrier, M. V.; Fontecilla-Camps, J. C.; Ghasemi, M.; Salmain, M. Artificial metalloenzymes derived from bovine β-lactoglobulin for the asymmetric transfer hydrogenation of an aryl ketone-synthesis, characterization and catalytic activity. *Dalton Trans* **2014**, *43*, 5482−5489.

(20) Ishii, T.; Tsuboi, S.; Sakane, G.; Yamashita, M.; Breedlove, B. K. Universal Spectrochemical series of Six-coordinate Octahedral Metal Complexes for Modifying the Ligand Field Splitting. *Dalton Trans* **2009**, *4*, 680−687.

(21) Bruce, M. I.; Costuas, K.; Davin, T.; Ellis, B. G.; Halet, J.-F.; Lapinte, C.; Low, P. J.; Smith, M. E.; Skelton, B. W.; Toupet, L. Iron versus Ruthenium: Dramatic Changes in Electronic Structure Result from Replacement of One Fe by Ru in [{Cp*(dppe)Fe}-CC-CC-{Fe(dppe)Cp*}]$^{n+}$ (n = 0, 1, 2). *Organometallics* **2005**, *24*, 3864−3881.

(22) Eskénazi, C.; Balavoine, G.; Meunier, F.; Rivière, H. Tuning of reactivity in epoxidation of alkenes by iron and ruthenium complexes associated to non-porphyrinic ligands. *J. Chem. Soc., Chem. Commun.* **1985**, 1111−1113.

(23) Fulmer, G. R.; Miller, A. J.; Sherden, N. H.; Gottlieb, H. E.; Nudelman, A.; Stoltz, B. M.; Bercaw, J. E.; Goldberg, K. I. NMR Chemical Shifts of Trace Impurities: Common Laboratory Solvents, Organics, and Gases in Deuterated Solvents Relevant to the Organometallic Chemist. *Organometallics* **2010**, *29*, 2176−2179.

(24) Kirsch, J. F.; Igelström, M. The Kinetics of the Papain-Catalyzed Hydrolysis of Esters of Carbobenzoxyglycine. Evidence for an Acyl-Enzyme Intermediate. *Biochemistry* **1966**, *5*, 783−791.

(25) Haquette, P.; Salmain, M.; Svedlung, K.; Martel, A.; Rudolf, B.; Zakrzewski, J.; Cordier, S.; Roisnel, T.; Fosse, C.; Jaouen, G. Cysteine-Specific, Covalent Anchoring of Transition Organomettalic Complexes to the Protein Papain from Carica papaya. *ChemBioChem* **2007**, *8*, 224−231.

(26) Riener, C. K.; Kada, G.; Gruber, H. J. Quick measurement of protein sulfhydryls with Ellman's reagent and with 4,4'-dithiodipyridine. *Anal. Bioanal. Chem.* **2002**, *373*, 266−276.

(27) Funk, M.; Nakagawa, Y.; Skochdopole, J.; Kaiser, E. Affinity Chromatographic Purification of Papain a Reinvestigation. *Int. J. Pept. Protein Res.* **1979**, *13*, 296−303.

(28) *SMART*, version 5.628; Bruker AXS Inc.: Madison, WI, 2001.

(29) *SAINT+*, version 6.22a; Bruker AXS Inc.: Madison, WI, 2001.

(30) Sheldrick, G. M. *SADABS*; University of Göttingen, Germany, 1996.

(31) Sheldrick, G. *Cell_Now (version 2008/1): Program for Obtaining Unit Cell Constants from Single Crystal Data*; University of Göttingen: Germany, 2008.

(32) Sheldrick, G. *Cell_Now and TWINABS*. University of Göttingen: Germany, 2008.

(33) *SHELXTL*, version 5.1; Bruker AXS Inc.: Madison, WI, 1997.

(34) Zhao, Y.; Truhlar, D. G. The M06 suite of density functionals for main group thermochemistry, thermochemical kinetics, noncovalent interactions, excited states, and transition elements: two new functionals and systematic testing of four M06-class functionals and 12 other functionals. *Theor. Chem. Acc.* **2008**, *120*, 215−241.

(35) Ehlers, A. W.; Böhme, M.; Dapprich, S.; Gobbi, A.; Höllwarth, A.; Jonas, V.; Köhler, K. F.; Stegmann, R.; Veldkamp, A.; Frenking, G. A Set of f-polarization Functions for Pseudo-potential basis sets of the Transition Metals Sc-Cu, Y-Ag and La-Au. *Chem. Phys. Lett.* **1993**, *208*, 111−114.

(36) Frisch, M. J.; Trucks, G. W.; Schlegel, H. B.; Scuseria, G. E.; Robb, M. A.; Cheeseman, J. R.; Scalmani, G.; Barone, V.; Mennucci, B.; Petersson, G. A.; Nakatsuji, H.; Caricato, M.; Li, X.; Hratchian, H. P.; Izmaylov, A. F.; Bloino, J.; Zheng, G.; Sonnenberg, J. L.; Hada, M.; Ehara, M.; Toyota, K.; Fukuda, R.; Hasegawa, J.; Ishida, M.; Nakajima, T.; Honda, Y.; Kitao, O.; Nakai, H.; Vreven, T.; Montgomery, J. A., Jr.; Peralta, J. E.; Ogliaro, F.; Bearpark, M.; Heyd, J. J.; Brothers, E.; Kudin, K. N.; Staroverov, V. N.; Kobayashi, R.; Normand, J.; Raghavachari, K.; Rendell, A.; Burant, J. C.; Iyengar, S. S.; Tomasi, J.; Cossi, M.; Rega, N.; Millam, J. M.; Klene, M.; Knox, J. E.; Cross, J. B.; Bakken, V.; Adamo, C.; Jaramillo, J.; Gomperts, R.; Stratmann, R. E.; Yazyev, O.; Austin, A. J.; Cammi, R.; Pomelli, C.; Ochterski, J. W.; Martin, R. L.; Morokuma, K.; Zakrzewski, V. G.; Voth, G. A.; Salvador, P.; Dannenberg, J. J.; Dapprich, S.; Daniels, A. D.; Farkas, O.; Foresman, J. B.; Ortiz, J. V.; Cioslowski, J.; Fox, D. J. *Gaussian 09*, revision D.01; Gaussian, Inc.: Wallingford, CT, 2009.